

~~CONFIDENTIAL~~

Copy
RM L51E01

206

NACA RM L51E01

~~53-34-27~~

NACA

DL4855



TECH LIBRARY KAFB, NM

RESEARCH MEMORANDUM

CONTRIBUTIONS OF WING, ⁰TAIL, AND FUSELAGE
TO THE AERODYNAMIC CHARACTERISTICS OF A SEMISPAN MODEL
OF A SUPERSONIC AIRPLANE CONFIGURATION AT TRANSONIC
SPEEDS FROM TESTS BY THE NACA WING-FLOW METHOD

By Norman S. Silsby and James M. McKay

Langley Aeronautical Laboratory
Langley Field, Va.

CLASSIFIED DOCUMENT

This document contains classified information affecting the National Defense of the United States within the meaning of the Espionage Act, USC 50-41 and 52. Its transmission or the revelation of its contents in any manner to an unauthorized person is prohibited by law.
Information so classified may be imparted only to persons in the military and naval services of the United States, appropriate civilian officers and employees of the Federal Government who have a legitimate interest therein, and to United States citizens of known loyalty and discretion who of necessity must be informed thereof.

NATIONAL ADVISORY COMMITTEE
FOR AERONAUTICS

WASHINGTON

July 11, 1951

~~CONFIDENTIAL~~

319. 21/13

~~2.237~~

7247

DATE _____

~~CONFIDENTIAL~~

NATIONAL ADVISORY COMMITTEE FOR AERONAUTICS

RESEARCH MEMORANDUM

CONTRIBUTIONS OF WING, TAIL, AND FUSELAGE
TO THE AERODYNAMIC CHARACTERISTICS OF A SEMISPAN MODEL
OF A SUPERSONIC AIRPLANE CONFIGURATION AT TRANSONIC
SPEEDS FROM TESTS BY THE NACA WING-FLOW METHOD

By Norman S. Silsby and James M. McKay

SUMMARY

An investigation has been made by the NACA wing-flow method at transonic speeds to determine the contributions of wing, tail, and fuselage to the aerodynamic characteristics of a semispan airplane model having a long slender fuselage and a straight wing and tail of low aspect ratio with faired symmetrical double-wedge airfoil sections 4.6 percent of the chord in thickness. Measurements were made of normal force, chord force, and pitching moment of the complete model, wing-fuselage combination, fuselage-tail combination, and fuselage alone. The tests were made at effective Mach numbers at the wing of the model from 0.60 to 1.13. The Reynolds number, based on wing mean aerodynamic chord, of the tests, ranged from about 0.3×10^6 to 0.7×10^6 .

The drag rise of the complete model occurred at a Mach number of about 0.90 for low values of normal-force coefficient; the peak of the drag rise occurred at a Mach number of 1.06. For the fuselage alone the drag rise occurred in a Mach number range from 0.97 to 1.10. The increase in drag coefficient with normal-force coefficient for the complete model was much greater than that for the induced-drag relation even at the lower Mach number of 0.7.

The aerodynamic-center location of the wing at low normal-force coefficients, as affected by wing-fuselage interaction effects, remained near 25 percent mean aerodynamic chord up to a Mach number of 0.9 and then moved back to almost 38 percent mean aerodynamic chord as the Mach number increased to 1.1. The aerodynamic-center position of the complete model was approximately constant at 42 percent mean aerodynamic chord as the Mach number increased to almost 1.0 and then moved back to about

~~CONFIDENTIAL~~PERMANENT
RECORD

2337

51 percent with further increase in Mach number to 1.1. At higher normal-force coefficients the rearward aerodynamic-center movement with Mach number was greater.

The rate of change of downwash at the tail with angle of attack $d\epsilon/d\alpha$ increased up to a Mach number of 1.0 and then decreased with further increase in Mach number. The experimental value of $d\epsilon/d\alpha$ and the rate of change of $d\epsilon/d\alpha$ with Mach number at a Mach number of 1.1 agreed closely with theoretical values for the wing alone.

INTRODUCTION

The present paper is the second of two papers on the results of tests to determine aerodynamic characteristics at transonic speeds of a semispan model of a supersonic airplane configuration. The first paper (reference 1) presented the longitudinal stability and control characteristics of the complete model. The present paper gives results of tests made to determine the contributions of wing, tail, and fuselage to the longitudinal stability characteristics of the semispan model. The model tested incorporated a very slender fuselage and low-aspect-ratio unswept wing and tail with thin sharp leading-edge airfoil sections. The horizontal tail of the model is of the all-movable type. Measurements were made of normal force, chord force, and pitching moment at various angles of attack for the following configurations: (1) complete model, (2) wing-fuselage, (3) fuselage-tail, and (4) fuselage alone. The tests covered a range of effective Mach numbers at the wing of the model from 0.60 to 1.13. The Reynolds number of the tests, based on the wing mean aerodynamic chord, ranged from about 0.3×10^6 to 0.7×10^6 .

SYMBOLS

M_L	local Mach number at wing surface of F-51D airplane
M_w	effective Mach number at wing of model
M_t	effective Mach number at tail of model
q_w	effective dynamic pressure at wing of model, pounds per square foot $\left(\frac{1}{2}\rho V^2\right)$

q_t	effective dynamic pressure at tail of model, pounds per square foot $\left(\frac{1}{2}\rho V^2\right)$
ρ	mass density of air, slugs per cubic foot
V	velocity, feet per second
c	local wing chord, inches
b	wing span, inches
S	wing area, semispan, square feet
y	spanwise coordinate, inches
\bar{c}	mean aerodynamic chord of wing; based on the relationship, inches $\int_0^{b/2} c^2 dy / \int_0^{b/2} c dy$
\bar{c}_t	mean aerodynamic chord of tail, inches
l_t	tail length, (center line of wing to center line of tail), inches
R_w	Reynolds number of wing based on \bar{c}
R_t	Reynolds number of tail based on \bar{c}_t
N	normal force, pounds
M	pitching moment, inch-pounds
D	drag force, resultant force parallel to local free-stream velocity, pounds
C_N	normal-force coefficient (N/qS)
$C_{m_{0.50\bar{c}}}$	pitching-moment coefficient referred to $0.50\bar{c}$ $(M/qS\bar{c})$

C_D	drag coefficient (D/qS)
C_{Di}	theoretical induced drag relation
A	aspect ratio
α	angle of attack of fuselage reference plane, degrees
i_t	incidence of horizontal stabilizer, degrees
$\frac{\Delta C_D}{\Delta C_N^2}$	drag factor
$\frac{\partial C_N}{\partial \alpha}$	rate of change of normal-force coefficient with angle of attack over linear portion of curve
$\left(\frac{\partial C_m}{\partial \alpha}\right)_{\alpha=0}$	rate of change of pitching-moment coefficient with angle of attack at zero angle of attack
$\left(\frac{\partial C_m}{\partial i_t}\right)_{\alpha=0}$	rate of change of pitching-moment coefficient with horizontal tail incidence at zero angle of attack
ϵ	downwash angle at tail, degrees
$\frac{d\epsilon}{dC_N}$	rate of change of downwash angle with normal-force coefficient
$\frac{d\epsilon}{d\alpha}$	rate of change of downwash angle with angle of attack

APPARATUS AND TESTS

The tests were made by the NACA wing-flow method, in which the model is mounted in the high-speed flow over the wing of an F-51D airplane.

Photographs of the semispan model equipped with an end plate at the fuselage center line are given as figures 1 and 2. The geometric

characteristics of the model are given in table I; other details of the model are shown in figure 3. A more complete description of the apparatus and methods of tests is given in reference 1.

In the present tests, continuous measurements were made of angle of attack, normal force, chord force, and pitching moment about the 50-percent-chord line of the wing as the model was oscillated through an angle-of-attack range of -3° to 11° and as the Mach number was increased steadily from 0.56 to 1.13. The configurations tested were the fuselage plus wing plus tail (hereinafter called the complete model), the wing-fuselage, the fuselage-tail, and the fuselage alone. The tail was always at 0° incidence. A test was also made to determine the tare drag of the end plate which was included in the configurations previously mentioned. The end plate was detached from the model and attached to the airplane wing surface with the same spacing from the surface as when it was attached to the model. The model was mounted as closely as practical (about 0.008 in.) to the end plate with provision made to indicate whether the model touched the end plate during the test. Thus, the drag of the model alone in the presence of the end plate was measured. The difference in drag between the model with and without end plate was taken to be the tare drag of the end plate. A free-floating vane, shown in figure 2, was used to determine the direction of air flow at the model location, as described in reference 2.

The chordwise velocity gradients in the test region of the airplane, as determined from static-pressure measurements at the wing surface with the model removed, are indicated in figure 4. The variation of Mach number at the tail M_t with Mach number at the wing M_w due to the chordwise velocity gradient is shown in figure 5. A more complete discussion of the method of determining the Mach number and dynamic pressure at the model can be found in references 1 and 2. The tests were made in three different altitude ranges to obtain different ranges of Reynolds number as described in reference 1. The variation of the average Reynolds number at the wing R_w and the average Reynolds number at the tail R_t with Mach number at the wing M_w for the three altitude conditions is shown in figure 6.

PRESENTATION OF RESULTS

A sample of the type of data obtained in the tests is given in figure 7. No correction for end-plate tare drag or buoyancy has been made to the data of this figure. In presenting the results in the subsequent figures the data points have been eliminated to avoid confusion and only the faired curves are shown. These faired curves represent averages of data obtained with increasing and decreasing

~~CONFIDENTIAL~~

angle of attack and also in different tests with varying Reynolds number (see fig. 6) since the variation of Reynolds number within the range covered had no significant effect.

Drag.- The results of the drag measurements are presented in figures 8 to 11. These drag results are corrected for end-plate tare drag and for buoyancy effects resulting from the pressure gradient in the test region. The variation of drag coefficient with Mach number at various normal-force coefficients is shown in figure 8 for the complete model and in figure 9 at various angles of attack for the fuselage alone. The variation of drag coefficient with normal-force coefficient at several Mach numbers for the complete model and fuselage alone is given in figure 10 together with the curve representing the subsonic induced-

drag relation $C_{D_i} = \frac{C_N^2}{\pi A}$. The variation of drag coefficient with the square of the normal-force coefficient $\frac{\Delta C_D}{\Delta C_N^2}$ as a function of Mach number is compared with the inverse of the lift-curve slope in figure 11.

Lift.- The variation of angle of attack with Mach number for several normal-force coefficients is shown for the complete model and wing-fuselage combination in figure 12, and the variation of normal-force coefficient with Mach number for several angles of attack of the fuselage alone is shown in figure 13. The lift-curve slopes $\partial C_N / \partial \alpha$ for the complete model, wing-fuselage combination, and fuselage alone are shown in figure 14 as a function of Mach number. Also included in figure 14 is the variation with Mach number of the effective lift-curve slope of the horizontal tail in the presence of the fuselage determined from pitching-moment data for the fuselage-tail and fuselage-alone configurations by the relation

$$\left(\frac{\partial C_N}{\partial \alpha} \right)_T = \left[\left(\frac{\partial C_m}{\partial \alpha} \right)_{F+T} - \left(\frac{\partial C_m}{\partial \alpha} \right)_F \right] \frac{S_w \bar{c} q_w}{S_t l_t q_t}$$

The results of the tare tests indicated that the end plate had no effect on the lift characteristics.

Pitching moment.- The results of pitching-moment measurements are shown in figures 15 to 17. The variation of pitching-moment coefficient with Mach number for various normal-force coefficients for the wing-fuselage configuration is given in figure 15, and for various angles of attack of the fuselage-tail and fuselage alone configurations in figures 16 and 17, respectively. Corresponding results for the complete

~~CONFIDENTIAL~~

model have been presented in reference 1 and are therefore not duplicated here. The pitching-moment slopes $\partial C_m / \partial \alpha$ as a function of Mach number are presented in figure 18 for the complete model (from data of reference 1), for the wing-fuselage and fuselage-tail combinations, and for the fuselage alone. The differences between the values of $\partial C_m / \partial \alpha$ for the fuselage-tail combination and fuselage alone, representing the effectiveness of the horizontal tail in the presence of the fuselage with varying angle of attack, is shown for comparison with $\partial C_m / \partial i_t$ (from data of reference 1), representing the effectiveness of the tail in the presence of the wing and fuselage but with varying tail angles at constant angle of attack. The aerodynamic-center position of the wing as affected by wing-fuselage interaction effects determined from

$$\frac{\left(\frac{\partial C_m}{\partial \alpha} \right)_{F+W} - \left(\frac{\partial C_m}{\partial \alpha} \right)_F}{\left(\frac{\partial C_N}{\partial \alpha} \right)_{F+W} - \left(\frac{\partial C_N}{\partial \alpha} \right)_F}$$

is given in figure 19. The aerodynamic-center position for the complete model

$$\frac{\left(\frac{\partial C_m}{\partial \alpha} \right)_{WFT}}{\left(\frac{\partial C_N}{\partial \alpha} \right)_{WFT}}$$

is also shown in figure 19. No correction to pitching moments for end-plate effects was indicated in tare tests.

Downwash.— The rate of change of downwash angle with normal-force coefficient $d\epsilon/dC_N$, and with angle of attack $d\epsilon/d\alpha$, are plotted against Mach number in figure 20. The procedure used to calculate these values involved the assumption that the downwash angle was equal to the sum of the tail incidence and the angle of attack at which the pitching moment for the particular tail incidence was equal to the pitching moment with tail off.

~~CONFIDENTIAL~~

DISCUSSION

Drag at zero lift or zero angle of attack.- The start of the drag rise for the complete model occurs at about a Mach number of 0.90 (fig. 8); whereas for the fuselage alone (fig. 9) the start of the drag rise occurs at a Mach number of about 0.97. The start of the drag rise for both configurations occurs at slightly lower Mach numbers at the higher normal-force coefficients or angles of attack. The total rise of drag coefficient for the complete model is about 0.026, and the peak of the drag rise occurs at a Mach number of about 1.06. For the fuselage alone the peak occurs at about the same Mach number as for the complete model and the increase in drag coefficient is about 0.009. The drag values for the fuselage and hence for the complete model are too high, possibly because of the low Reynolds number and half-model test method. However, other wing-flow tests of a body (unpublished data) indicated that near zero lift the variation in drag coefficient with Mach number was in reasonable agreement with the results of free-fall tests of a similar body. The difference in drag coefficient between the complete model and the fuselage alone gives a rise in drag coefficient for the wing and tail of 0.018 based on total exposed area of wing and tail.

Variation of drag with lift.- The increase in drag coefficient with normal-force coefficient for the complete model (fig. 10) is much greater than for the induced-drag relation $C_{D_i} = \frac{C_N^2}{\pi A}$ even at the lowest Mach number of the tests ($M = 0.7$). The values of $\Delta C_D / \Delta C_N^2$ are lower than those of the inverse of the lift-curve slope $\frac{1}{57.3 \frac{\partial C_N}{\partial \alpha}}$ at least up to

a Mach number of 0.975 (fig. 11). This indicates that there is some leading-edge suction present, and the resultant force due to angle of attack is acting somewhat forward of the normal to the wing chord. At Mach numbers from 0.975 to 1.05, the values of $\Delta C_D / \Delta C_N^2$ agree with the inverse of the lift-curve slope, indicating that the resultant force due to angle of attack is acting normal to the chord of the wing in this Mach number range. This can possibly be explained by the fact that as the flow approaches sonic speed it begins to expand around the sharp leading edge of the wing, eliminating the subsonic separated region, and thence the suction at the leading edge.

Lift (complete model, wing-fuselage, tail).- The variation of the angle of attack with Mach number for a given normal-force coefficient is similar for the complete model and wing-fuselage configurations at values of normal-force coefficient below 0.6 (fig. 12). At the angle

~~CONFIDENTIAL~~

of attack corresponding to $C_N = 0.6$, the wing-fuselage configuration is beginning to stall at a Mach number less than 0.76, whereas at the same values of normal-force coefficient, the complete model (at a lower angle of attack because of the added lift of the tail) has not yet started to stall. The normal-force coefficients for the fuselage alone were relatively unaffected by Mach number at all the angles of attack tested (fig. 13).

The variations of the lift-curve slope with Mach number for the complete model and for the wing-fuselage combination are quite similar (fig. 14). Both increase at about the same rate up to a Mach number of 0.95 and then decrease somewhat as the Mach number is increased to 1.1. As indicated by the difference in level of the two curves, the tail contributes about 10 percent to the lift of the complete model. The lift produced by the fuselage alone is small (about 4 percent of that for the complete model) and does not vary appreciably with Mach number.

The variation of the effective lift-curve slope of the tail with Mach number, which includes tail-fuselage interaction effects, is quite similar to those for the complete model and wing-fuselage combination except that the peak occurs at a slightly lower Mach number, probably as a result of the higher Mach number at the tail relative to that at the wing (see fig. 5). Although the tail has the same configuration as the wing, the lift-curve slope of the tail is 20 to 25 percent less than that for the wing (wing-fuselage less fuselage). Part of this difference may be due to tail-fuselage interaction effects but it also may be attributable to the fact that the tail is partly submerged in the boundary layer over the test section which is relatively deep in relation to the small tail size.

Pitching moment.— The pitching moments for the wing-fuselage and fuselage-tail combinations show little variation with Mach number for normal-force coefficients and angles of attack near zero (figs. 15 and 16). At higher normal-force coefficients or angles of attack, there was considerable variation in pitching moment with Mach number, reflecting the variation in $\partial C_N / \partial \alpha$ of the tail (fig. 14) and aerodynamic center of the wing (fig. 19) with Mach number (at least up to $C_N = 0.4$) but the variations are quite regular. The rate of change of pitching-moment coefficient with normal-force coefficient or the aerodynamic-center location of the wing-fuselage does not appear to vary with normal-force coefficient at Mach numbers below about 0.85 (until stalling begins near $C_N = 0.6$) but at higher Mach numbers shows a continuous rearward movement as the normal-force coefficient is increased (fig. 15). At a Mach number of 1.1 the change in aerodynamic center amounts to about 0.20c with a change in C_N from 0 to 0.6. The pitching moments for the

fuselage alone were relatively unaffected by Mach number at all angles of attack tested (fig. 17).

The contributions of the various components to the stability in terms of $\partial C_m / \partial \alpha$ are presented in figure 18. It appeared that the value of $\partial C_m / \partial \alpha$ due to the tail (in the absence of downwash from the wing) was more negative when determined as the difference between the values of $\partial C_m / \partial \alpha$ of the tail-fuselage combination and fuselage alone, than the values of dC_m / di_t obtained with the complete model, although the variation with Mach number is quite similar. The actual extent of the effects of the presence of the wing (other than downwash) and the effects of the fuselage on the stability contribution of the tail were not determined. However, the fact that the variation of lift-curve slope of the tail with Mach number (fig. 14), deduced from these results, is similar to that for the complete model or wing-fuselage combination suggests that the tail contribution is not greatly affected by any variations in these interaction effects with Mach number. The difference between $\partial C_m / \partial \alpha$ for the wing-fuselage, and for the fuselage alone, representing the contribution of the wing plus wing-fuselage interaction effects, increases somewhat up to a Mach number of 0.9 and thereafter decreases up to a Mach number of 1.1 (fig. 18). In terms of aerodynamic-center location (fig. 19) it is found that the aerodynamic center remains near the quarter-chord point up to a Mach number of 0.9 and then moves back with increasing Mach number to about 38-percent \bar{c} at a Mach number of 1.075. As mentioned previously, this rearward movement of aerodynamic center with Mach number becomes greater at higher normal-force coefficients. The complete model is unstable about an axis through the 50-percent mean-aerodynamic-chord position at Mach numbers below about 1.08 and becomes stable at Mach numbers between 1.08 and 1.1. This variation corresponds approximately to a constant aerodynamic-center position of 42-percent \bar{c} up to a Mach number of almost 1.0, and then a rearward movement to 51-percent \bar{c} at a Mach number of 1.1.

Downwash.— The variation with Mach number of the rate of change of downwash angle at the tail with angle of attack $d\epsilon / d\alpha$ and with normal-force coefficient $d\epsilon / dC_N$ are shown in figure 20. The data show that $d\epsilon / d\alpha$ increased gradually from 0.58 to a maximum value of 0.66 at a Mach number of 1.0 and then decreased at higher Mach numbers to a value of 0.5 at $M = 1.1$. The value of $d\epsilon / dC_N$ decreased gradually from a Mach number of 0.7 to 1.0, and then decreased at a more rapid rate in the Mach number range from 1.0 to 1.1. A theoretical calculation of rate of change of downwash angle with angle of attack at supersonic speeds was made according to the method of Lagerstrom and Graham (reference 3) on a rectangular wing with the same area and mean aerodynamic chord as the tapered wing of the present tests but with resulting slightly lower span and aspect ratio. The variation with Mach number of this

theoretical $d\epsilon/d\alpha$ is plotted in figure 20 for comparison with the results of the present tests. The theoretical variation of $d\epsilon/d\alpha$ with Mach number has the same general trend beyond a Mach number of 1.1 as the experimental values have between 1.0 and 1.1, and at $M = 1.1$, the theoretical value of $d\epsilon/d\alpha$ agrees closely with the experimental value. The downwash measurements include some effects of the flow around the fuselage, whereas the theoretical calculations do not.

CONCLUDING REMARKS

The start of the drag rise of the complete model occurred at a Mach number of about 0.90 for low normal-force coefficients; the total rise of drag coefficient for the complete model was about 0.026, and the peak of the drag rise occurred at a Mach number of 1.06. For the fuselage alone the drag rise occurred between a Mach number of 0.97 and 1.10 and amounted to 0.009. The increase in drag coefficient with normal-force coefficient for the complete model is much greater than for the induced-drag relation even at the lower Mach number of 0.7.

The aerodynamic-center location of the wing at low normal-force coefficients, as affected by wing-fuselage interaction effects, remained near 25 percent mean aerodynamic chord up to a Mach number of 0.9 and then moved back to almost 38 percent mean aerodynamic chord as the Mach number increased to 1.1. The aerodynamic-center position of the complete model was approximately constant at 42 percent mean aerodynamic chord as the Mach number increased to almost 1.0 and then moved back to about 51 percent with further increase in Mach number to 1.1. At higher normal-force coefficients the rearward aerodynamic-center movement with Mach number was greater.

Any variation of interaction effects between the wing and tail (other than downwash) with Mach number or between the fuselage and tail was apparently not large enough to affect appreciably the variation with Mach number of the tail's contribution to the stability of the model.

The rate of change of downwash at the tail with angle of attack $d\epsilon/d\alpha$ increased up to a Mach number of 1.0 and then decreased with further increase in Mach number. The experimental value of $d\epsilon/d\alpha$ and the rate of change of $d\epsilon/d\alpha$ with Mach number at a Mach number of 1.1 agreed closely with theoretical values for the wing alone.

Langley Aeronautical Laboratory
National Advisory Committee for Aeronautics
Langley Field, Va.

~~CONFIDENTIAL~~

NACA RM L51E01

REFERENCES

1. Silsby, Norman S., and McKay, James M.: Longitudinal Stability and Control Characteristics of a Semispan Model of a Supersonic Airplane Configuration at Transonic Speeds from Tests by the NACA Wing-Flow Method. NACA RM L8G30, 1948.
2. Johnson, Harold I.: Measurements of Aerodynamic Characteristics of a 35° Sweptback NACA 65-009 Airfoil Model with $\frac{1}{4}$ -Chord Plain Flap by the NACA Wing-Flow Method. NACA RM L7F13, 1947.
3. Lagerstrom, P. A., and Graham, Martha E.: Linearized Theory of Supersonic Control Surfaces. Jour. Aero. Sci., vol. 16, no. 1, Jan. 1949, pp. 31-34.

~~CONFIDENTIAL~~

TABLE I

GEOMETRIC CHARACTERISTICS OF SEMISPAN MODEL OF
SUPERSONIC AIRPLANE CONFIGURATION

Wing:

Section	Faired double wedge
Thickness-chord ratio, percent	4.6
Semispan, inches	3.44
Mean aerodynamic chord, inches	1.79
Chord at tip, inches	1.15
Chord at plane of symmetry, inches	2.30
Area (semispan), square inches	5.94
Aspect ratio	4.0
Taper ratio	2:1
Dihedral, degrees	0
Incidence, degrees	0

Horizontal Tail:

Section	Faired double wedge
Thickness-chord ratio, percent	4.6
Semispan, inches	1.75
Mean aerodynamic chord, inches89
Chord at tip, inches57
Chord at plane of symmetry, inches	1.15
Area (semispan), square inches	1.50
Aspect ratio	4.0
Taper ratio	2:1
Dihedral, degrees	10

Fuselage length, inches 14.15

Tail length (center line of wing to center line
of tail), inches 5.74





Figure 1.- Semispan model of supersonic airplane configuration.

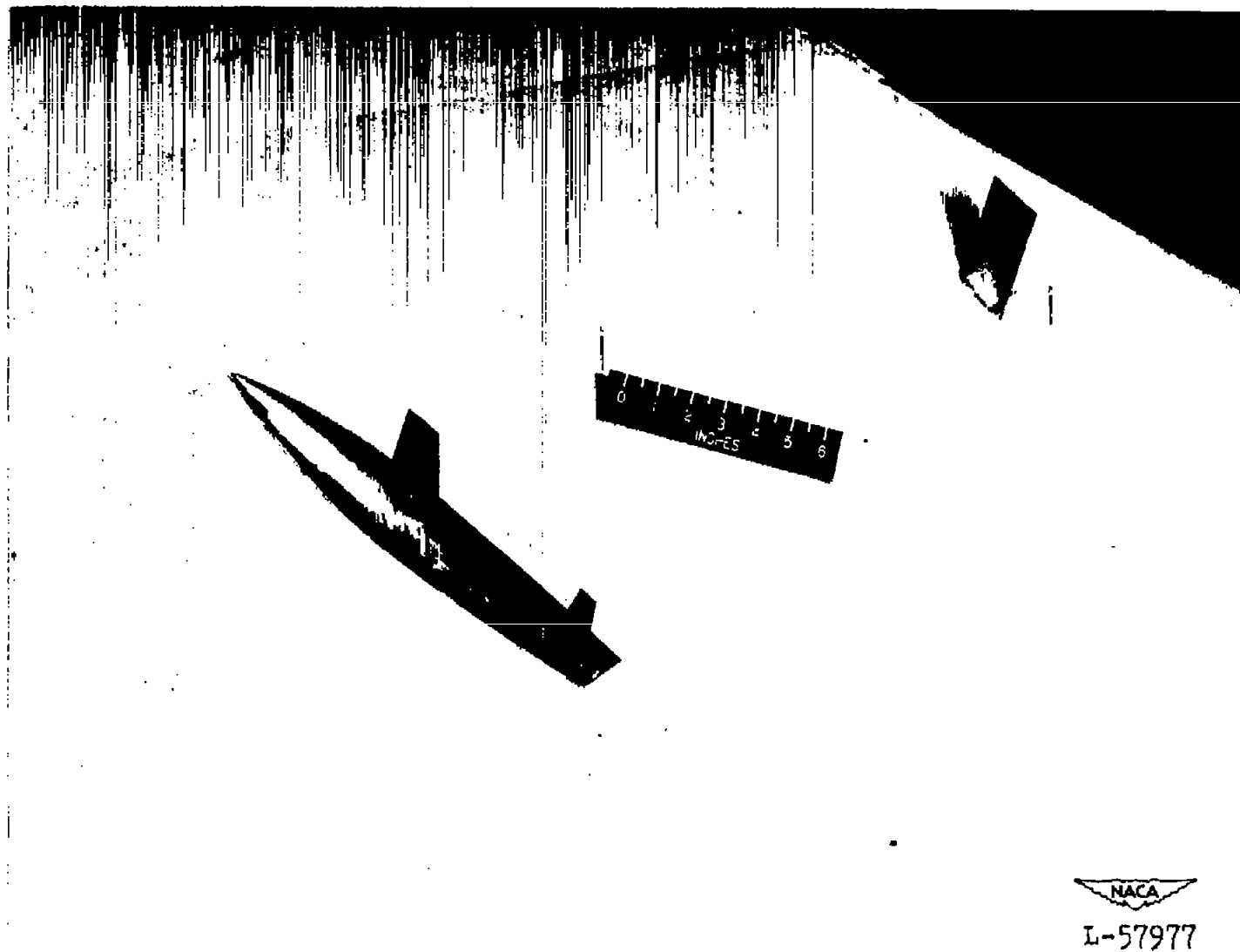


Figure 2.- Semispan supersonic airplane model mounted on wing of F-51D airplane. Free-floating vane also shown.

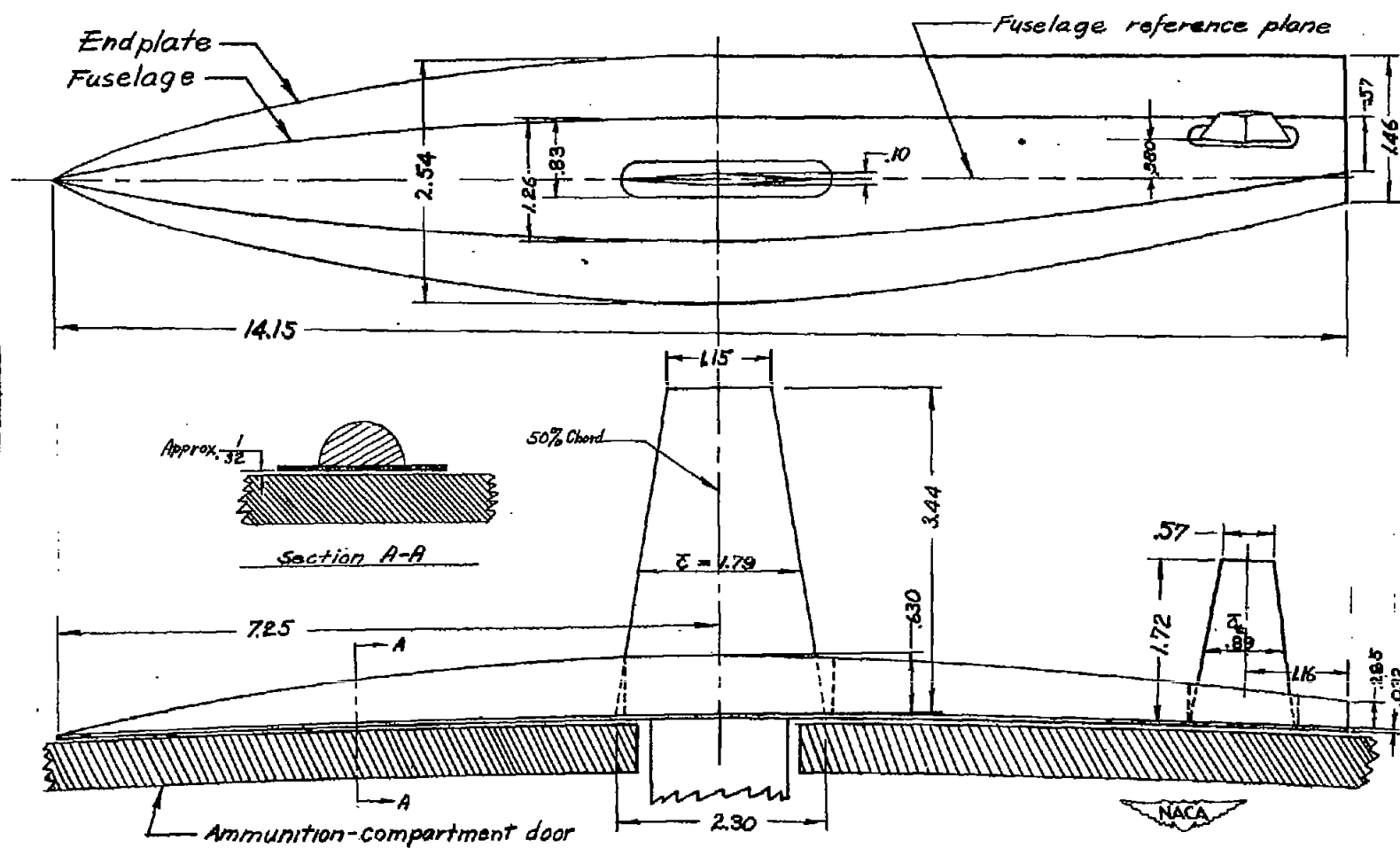


Figure 3.- Details of semispan model of supersonic airplane configuration.
(All dimensions are in inches.)

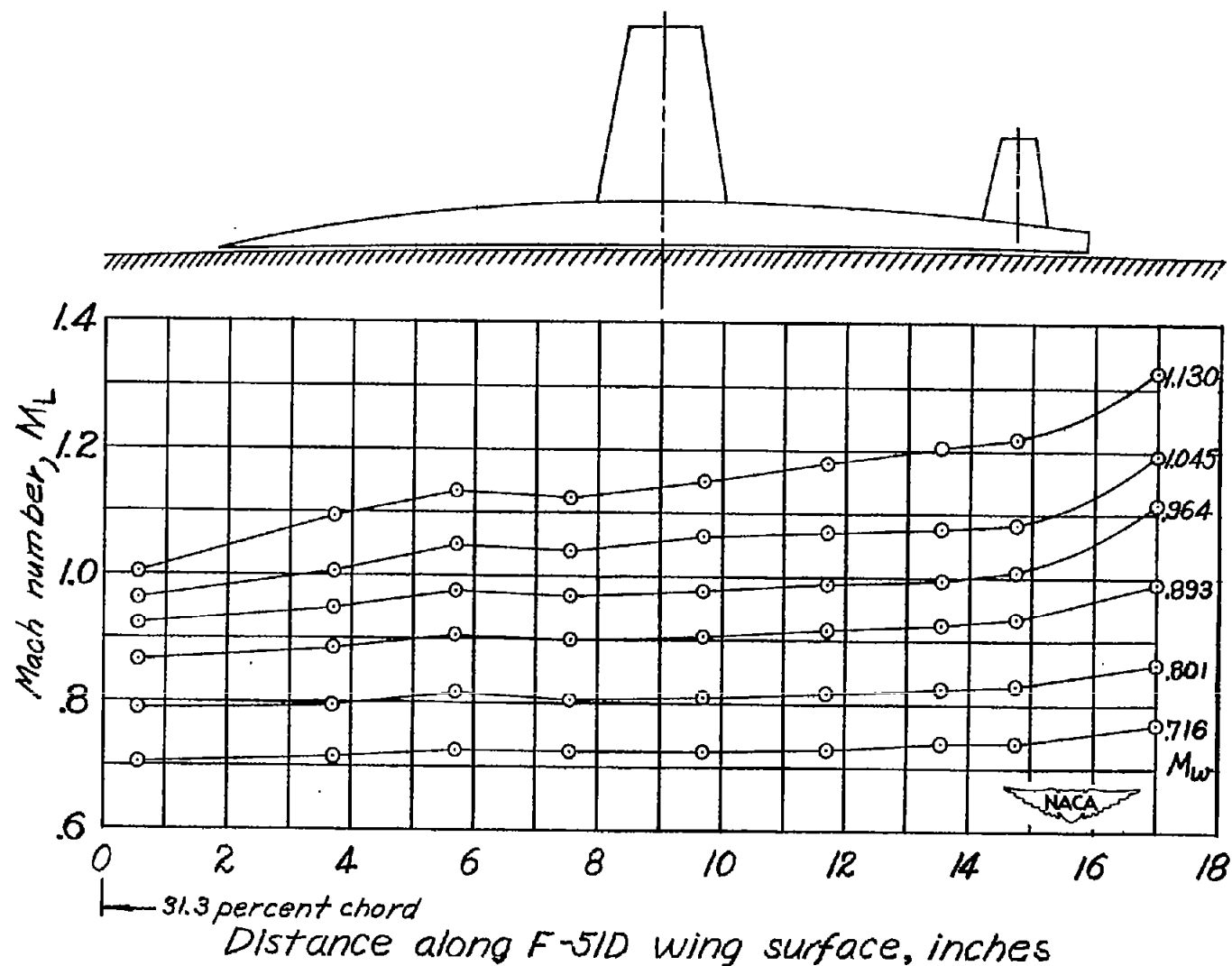


Figure 4.- Typical chordwise variation of Mach number in the test region on the surface of the airplane wing for several Mach numbers at the wing of the model. Chordwise location of model also shown.

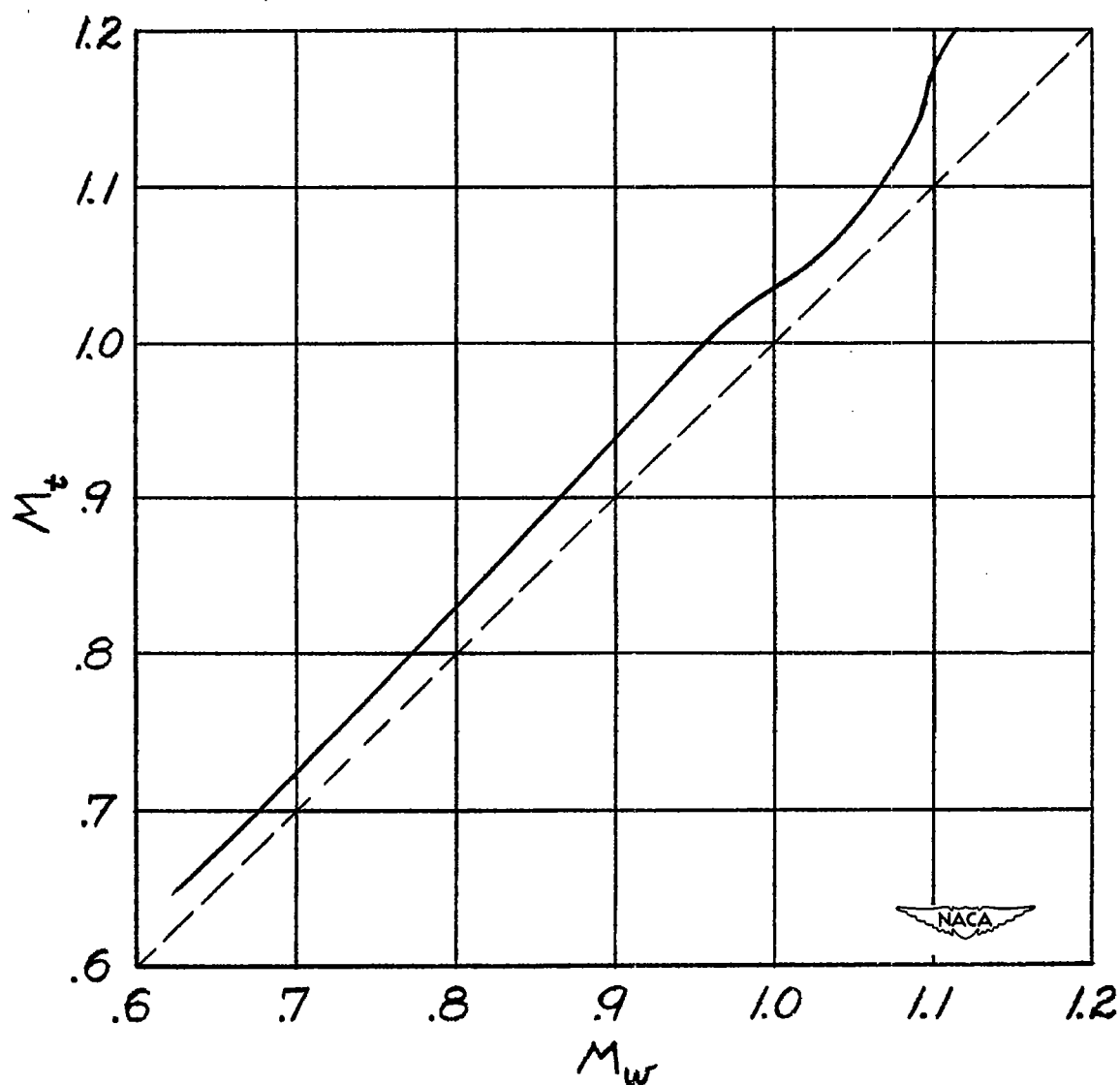


Figure 5.- Variation of Mach number at the tail M_t with Mach number at the wing M_w . Line of agreement shown dashed.

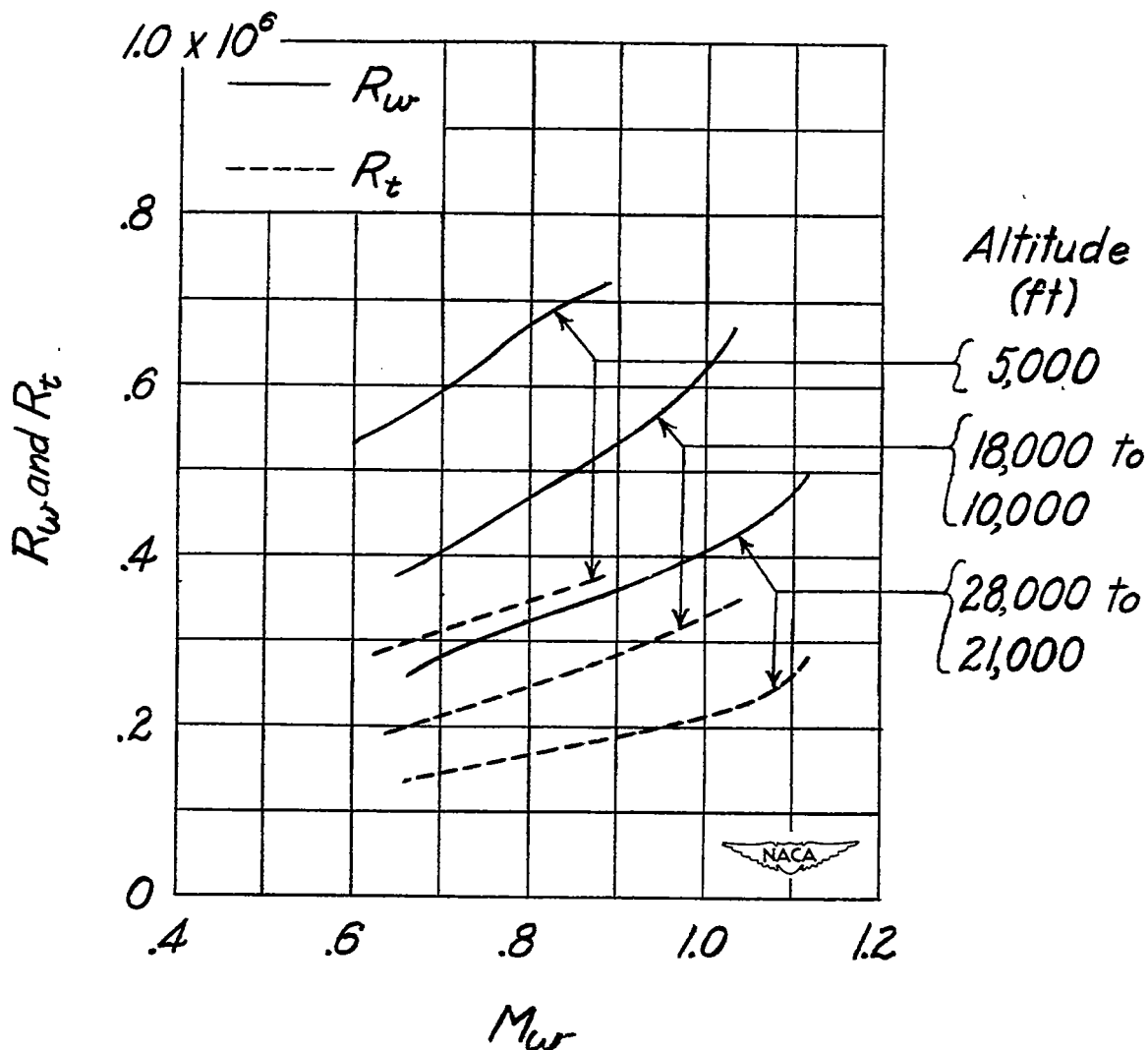


Figure 6.- Variation of Reynolds number of wing R_w and Reynolds number of tail R_t with Mach number for tests at three ranges of altitude.

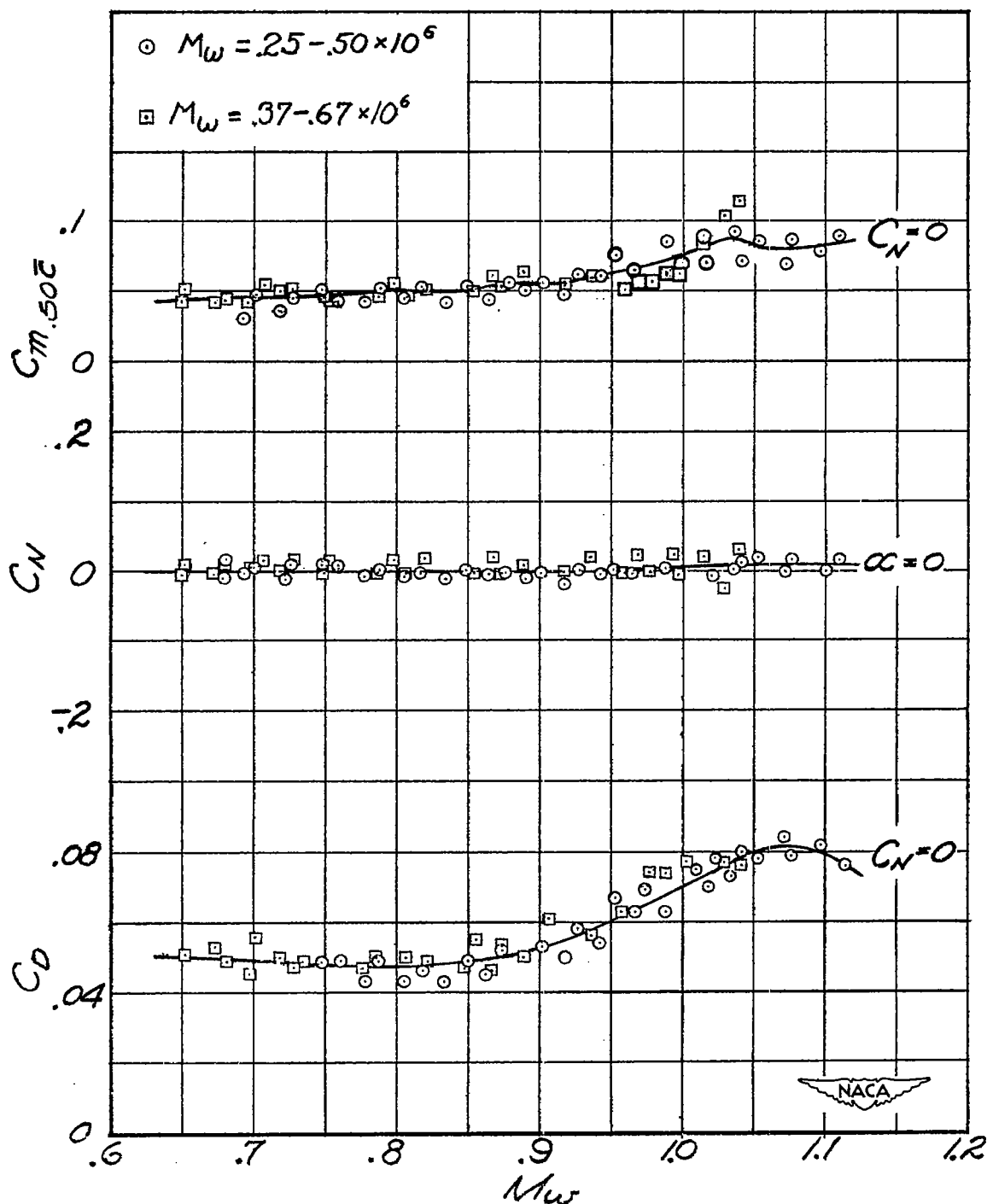


Figure 7.- Typical data showing pitching-moment coefficient and drag coefficient at $C_N = 0$, and also normal-force coefficient at $\alpha = 0$ for the complete model for two ranges of Reynolds numbers.

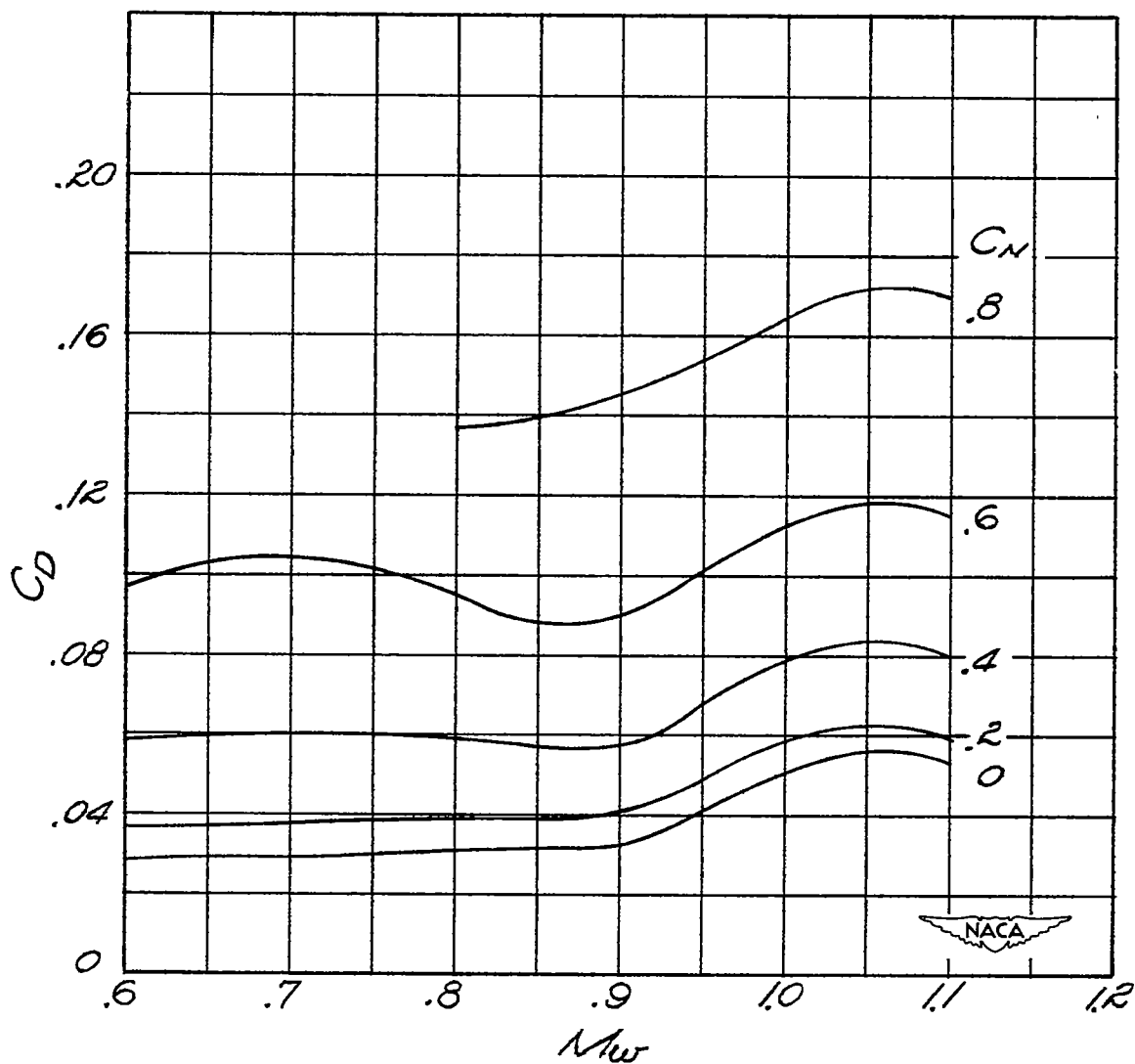


Figure 8.- Variation of the drag coefficient with Mach number for the complete model for various normal-force coefficients. $i_t = 0^\circ$.

~~CONFIDENTIAL~~

NACA RM L51E01

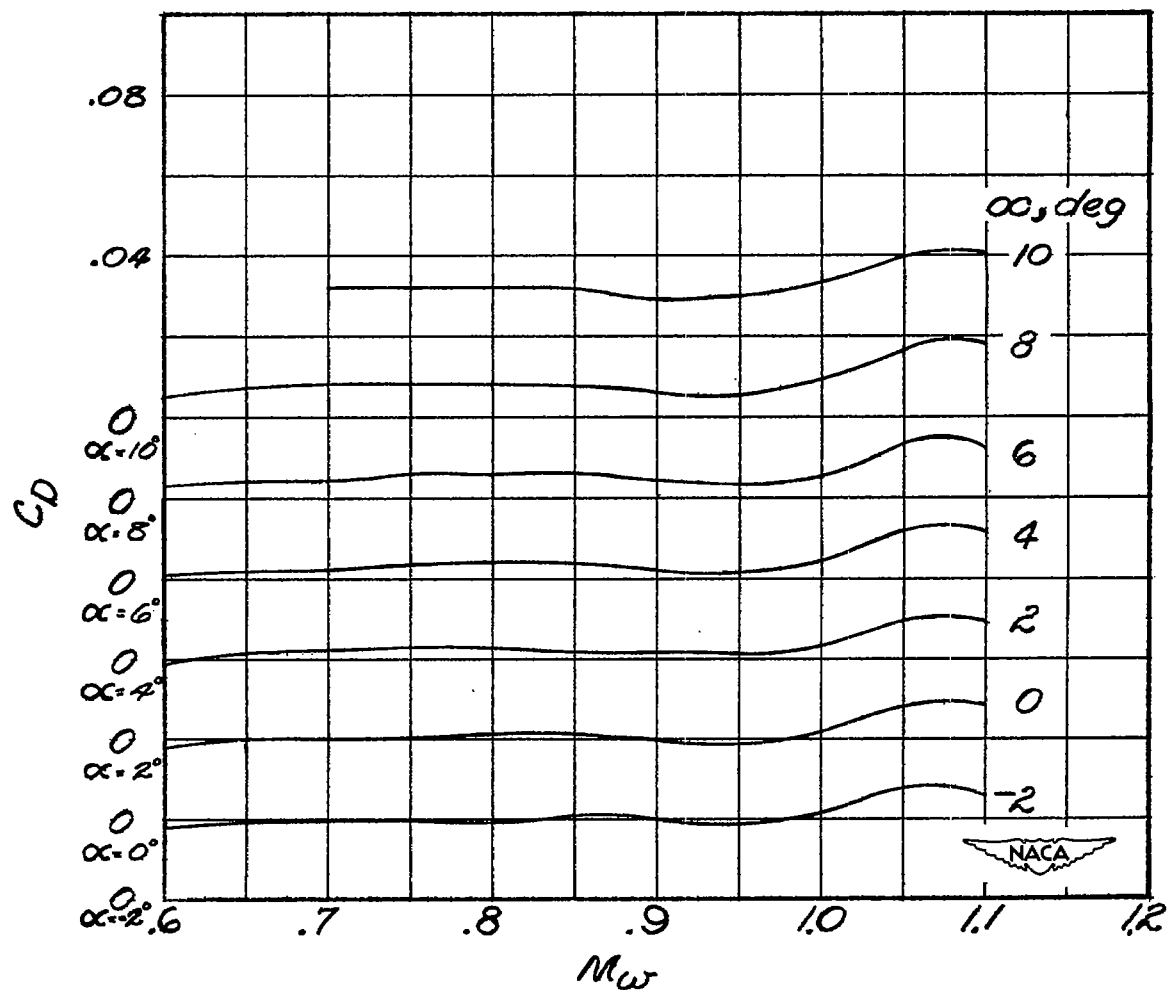


Figure 9.- Variation of drag coefficient with Mach number of the fuselage alone for various angles of attack.

~~CONFIDENTIAL~~

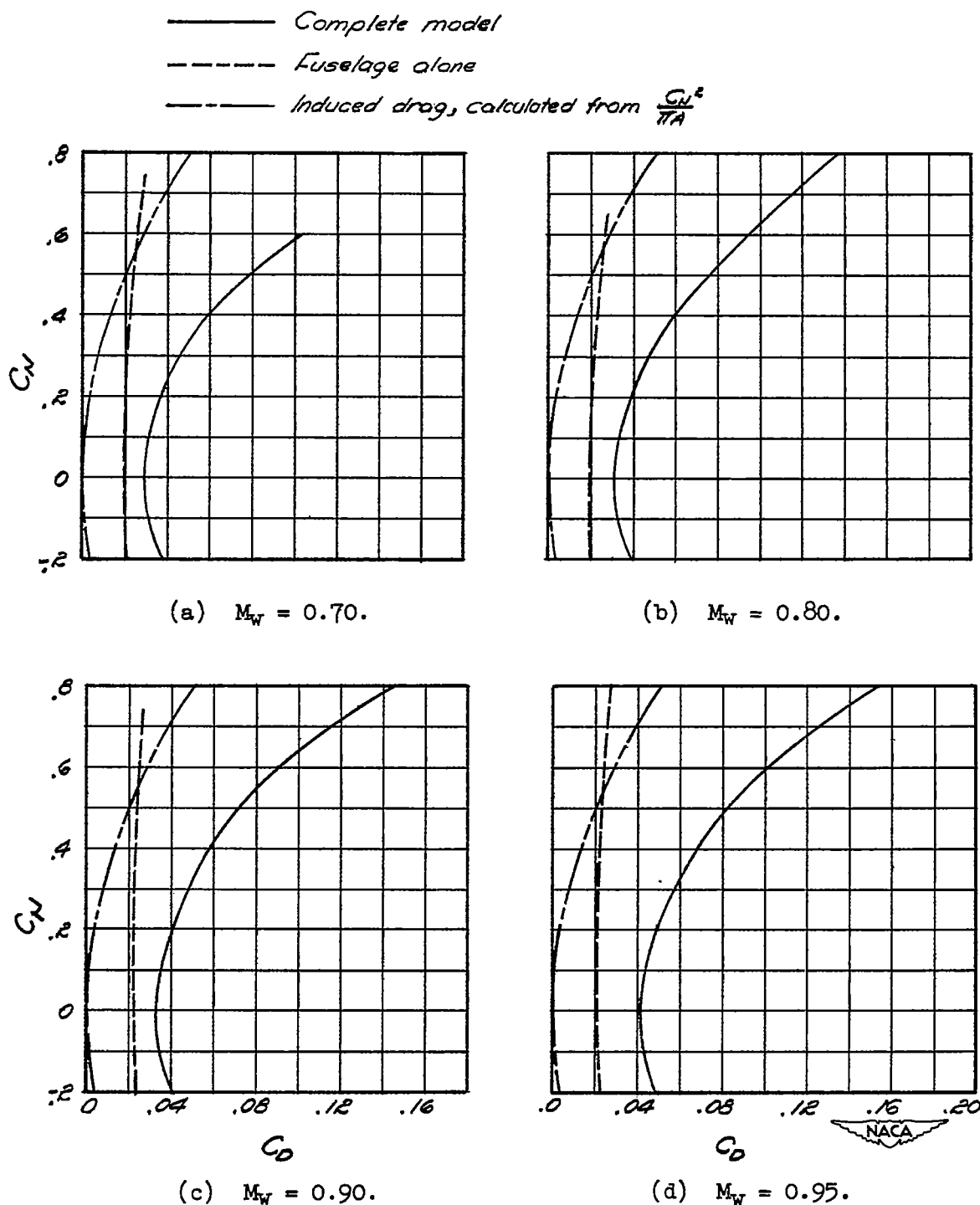


Figure 10.- Variation of normal-force coefficient with drag coefficient at several Mach numbers for the complete model ($i_t = 0^\circ$) and for the fuselage alone. Theoretical induced drag also shown for comparison.

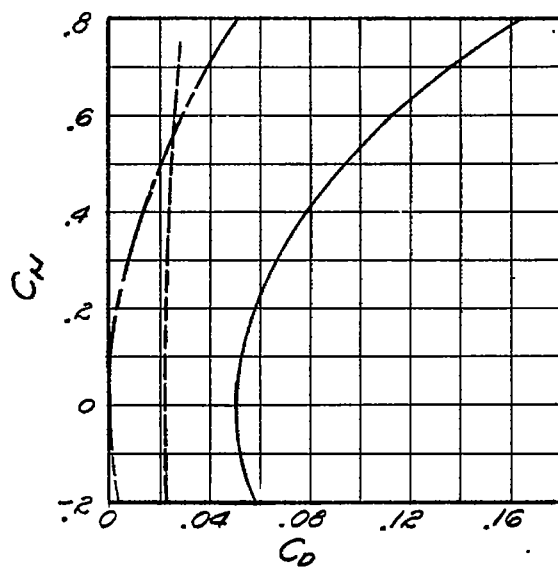
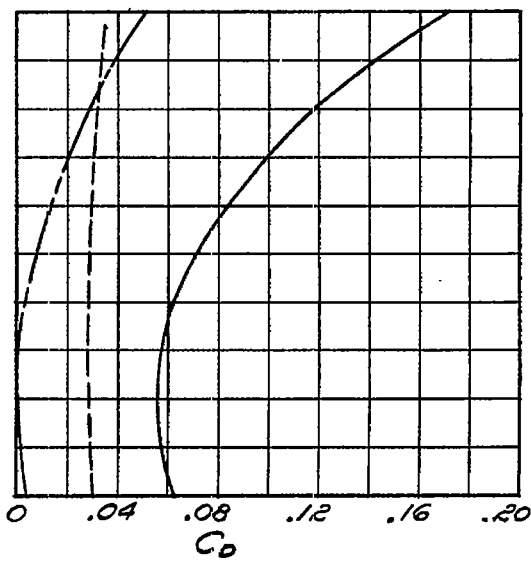
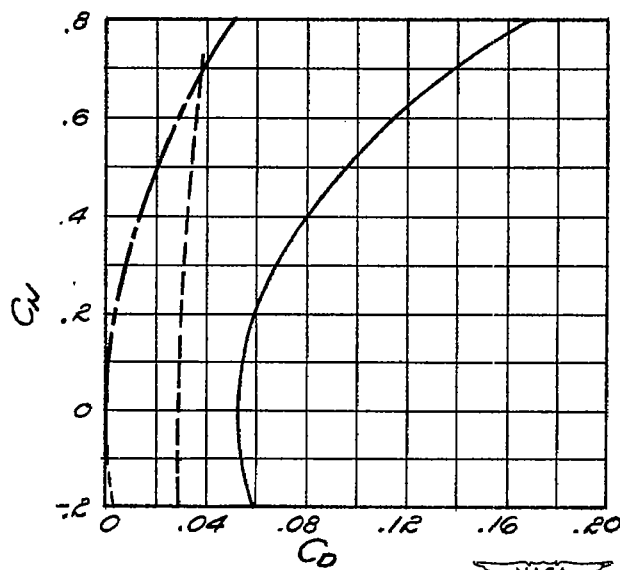
~~CONFIDENTIAL~~(e) $M_W = 1.00$.(f) $M_W = 1.05$.(g) $M_W = 1.10$.

Figure 10.- Concluded.

~~CONFIDENTIAL~~

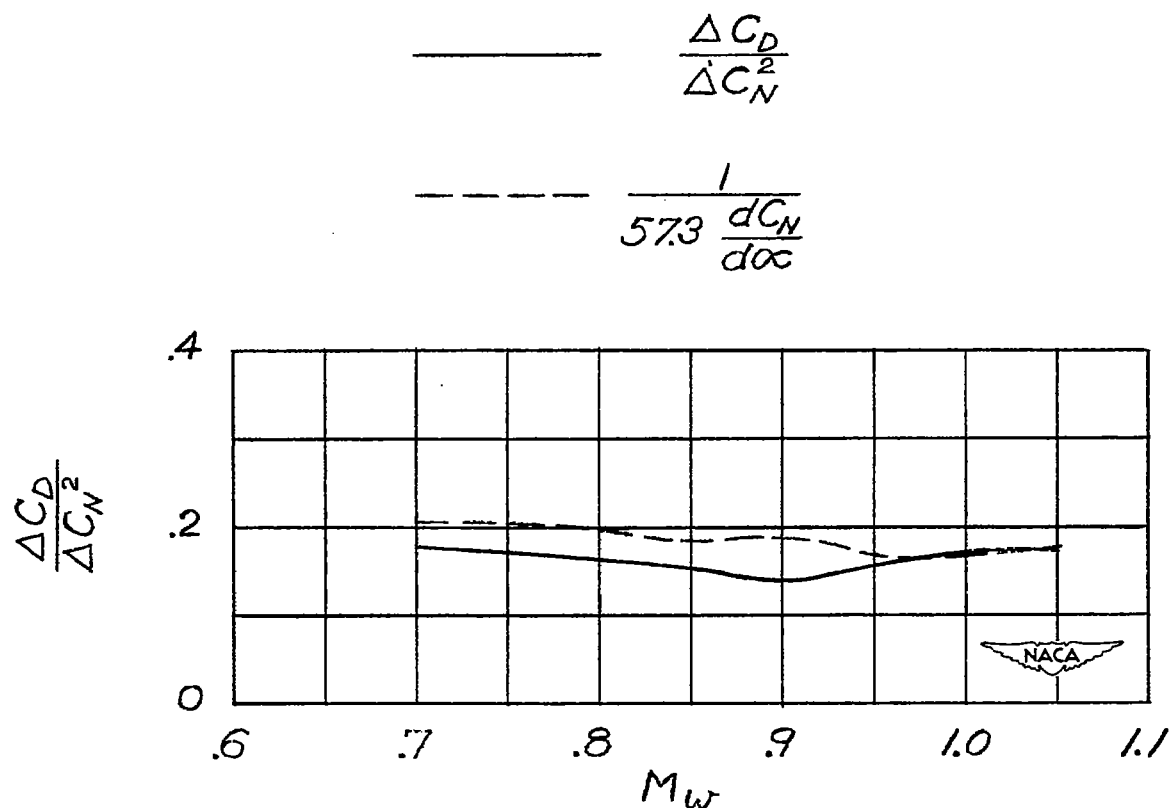


Figure 11.- The variation of the factor $\frac{\Delta C_D}{\Delta C_N^2}$ with Mach number and the inverse of the lift-curve slope for the complete model.

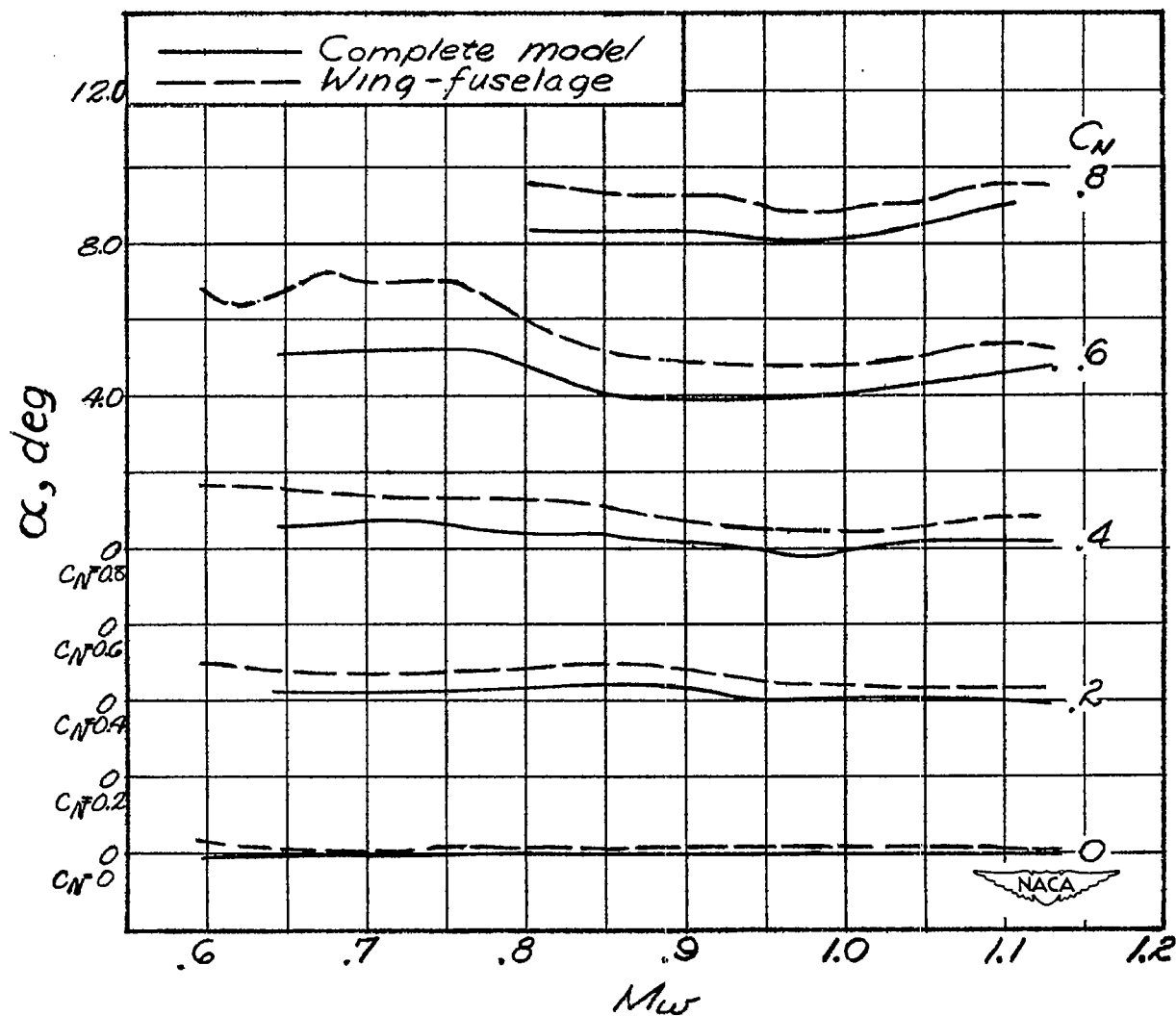


Figure 12.- Variation of angle of attack with Mach number for several normal-force coefficients for the complete model ($i_t = 0^\circ$) and for the wing-fuselage combination.

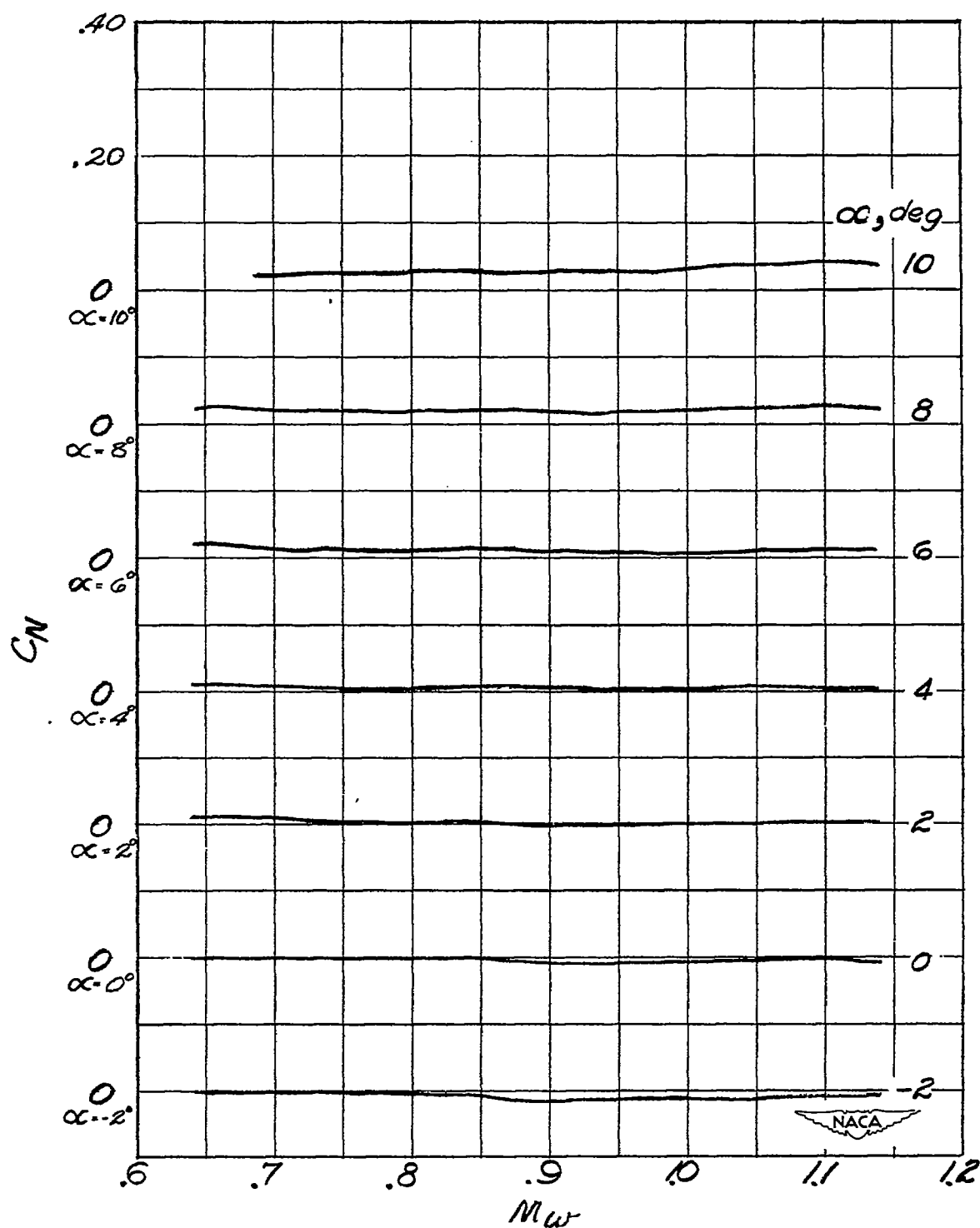


Figure 13.- Variation of normal-force coefficient with Mach number for the fuselage alone at several angles of attack.

~~CONFIDENTIAL~~

NACA RM L51E01

W Wing
F Fuselage
T Tail

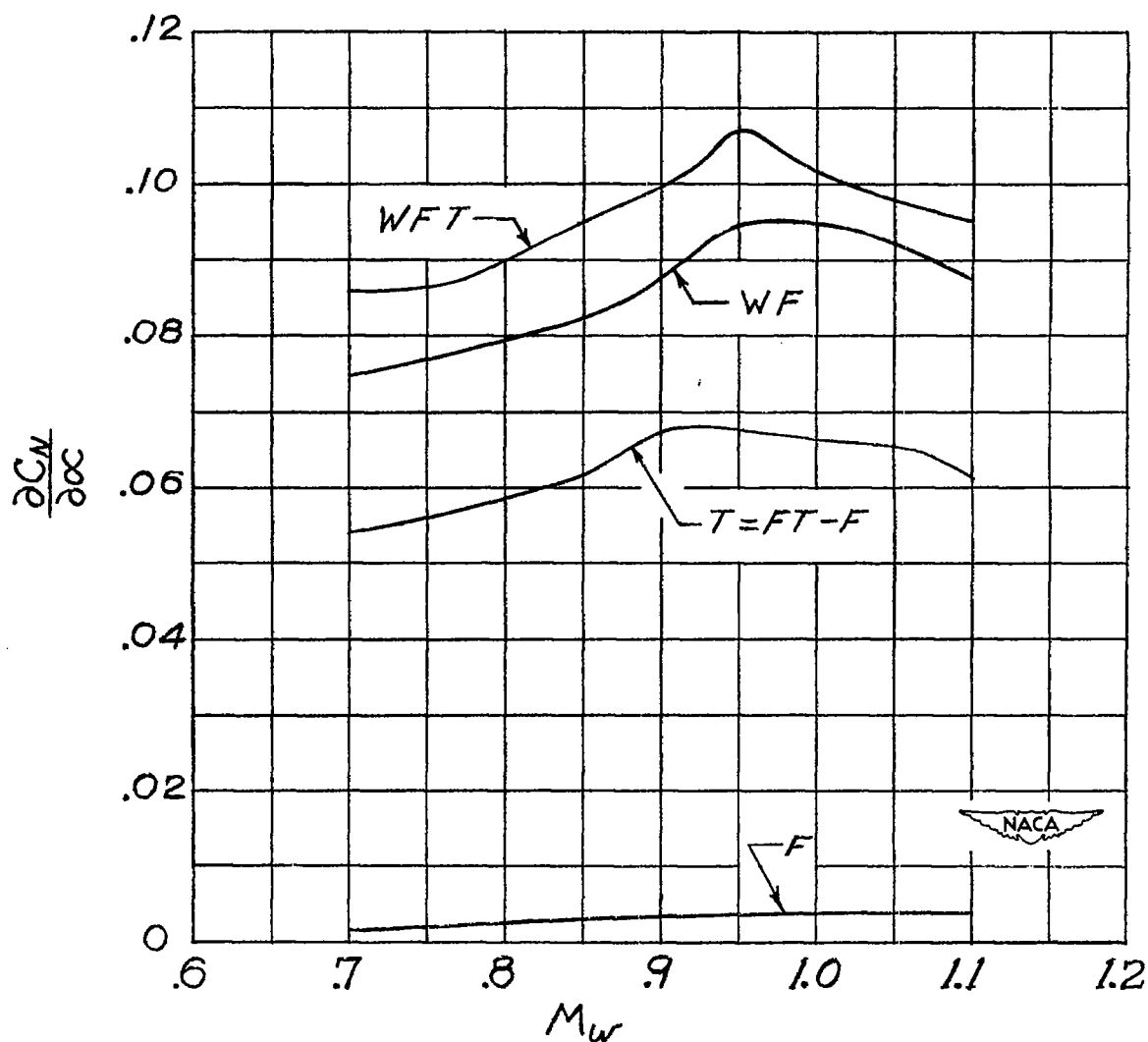


Figure 14.- Variation with Mach number of rate of change of normal-force coefficient with angle of attack for various configurations. C_N range 0. to 0.4 for complete model and wing-fuselage combination; $C_N \approx 0$ for fuselage alone.

~~CONFIDENTIAL~~

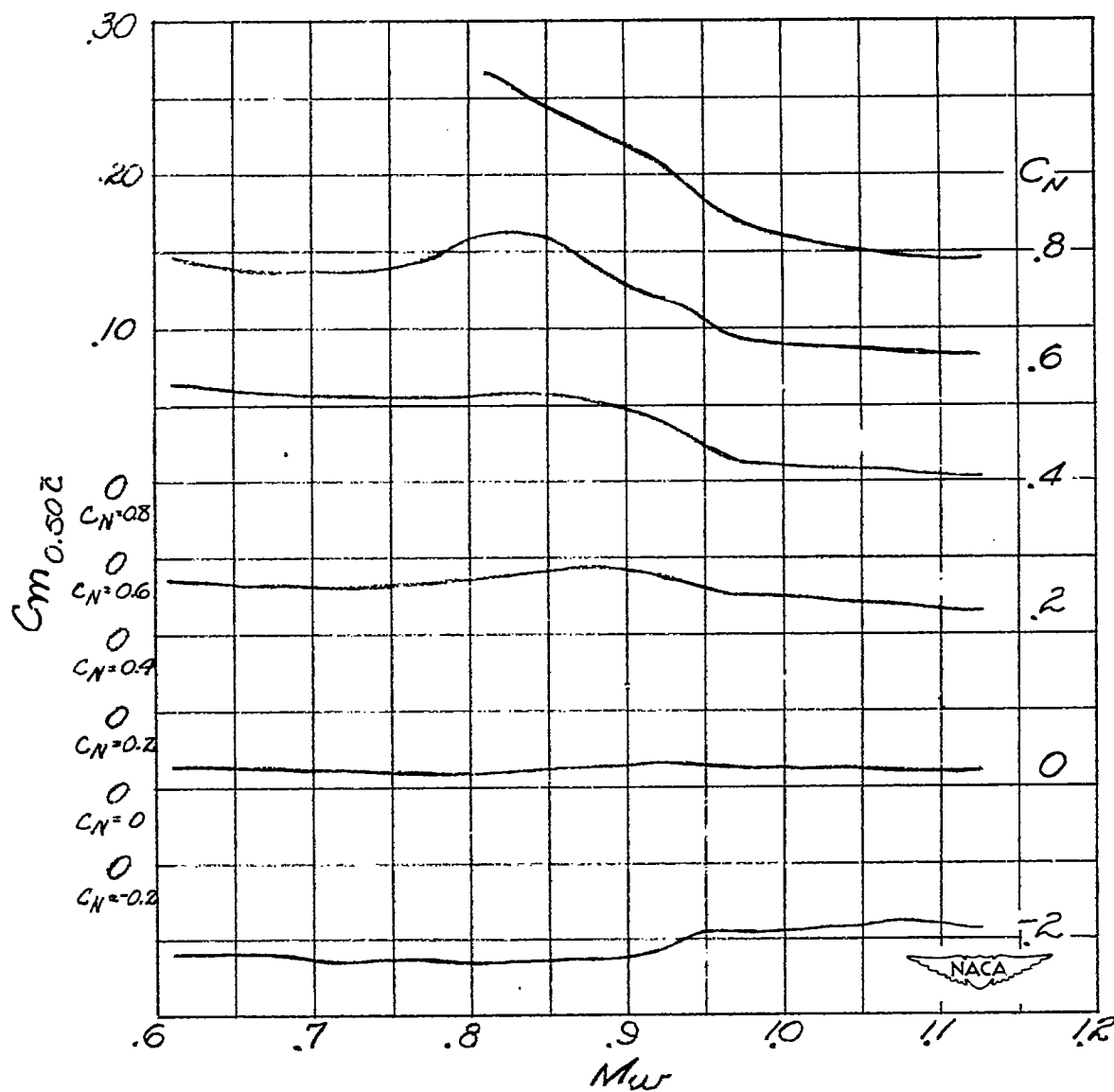


Figure 15.- Variation of pitching-moment coefficient with Mach number for the wing-fuselage configuration at several normal-force coefficients.

~~CONFIDENTIAL~~

NACA RM L51E01

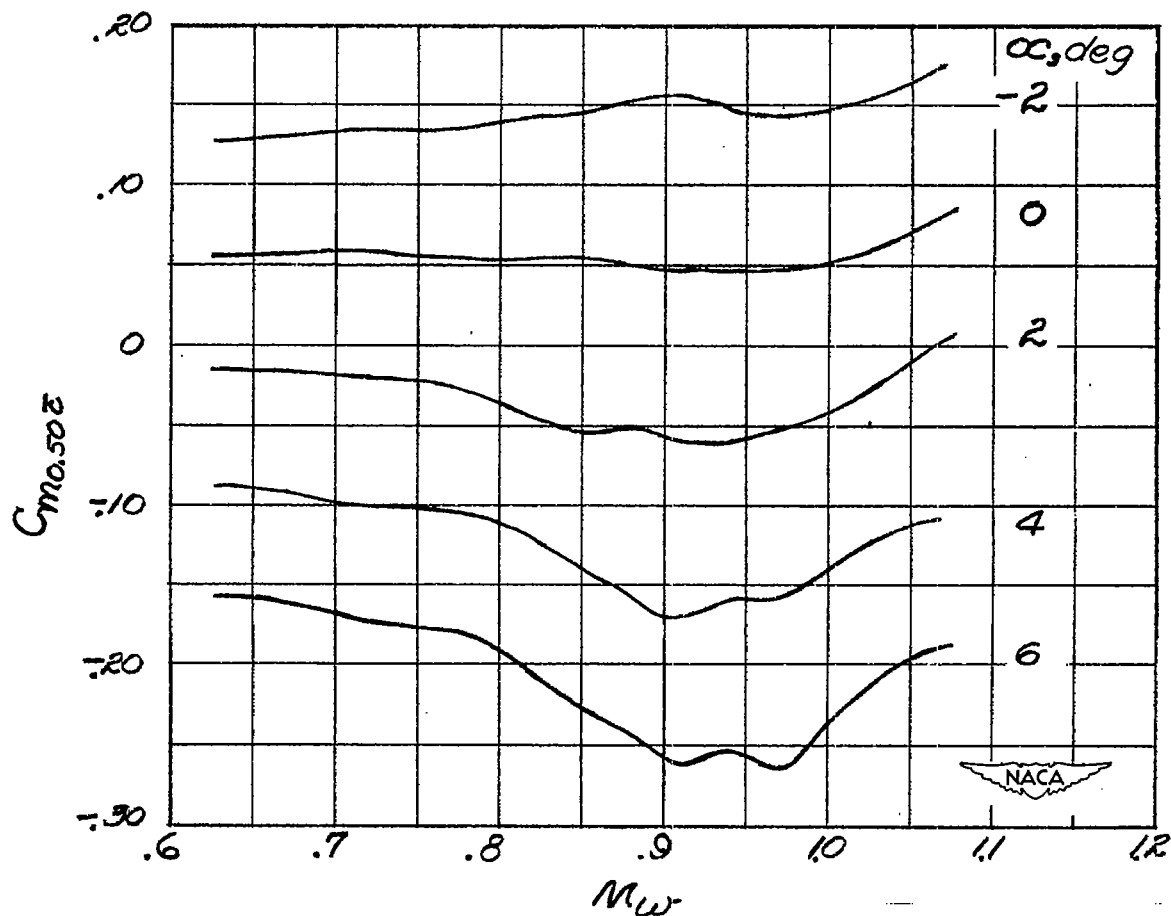


Figure 16.- Variation with Mach number of pitching-moment coefficient for fuselage-tail configuration at various angles of attack. $i_t = 0^\circ$.

~~CONFIDENTIAL~~

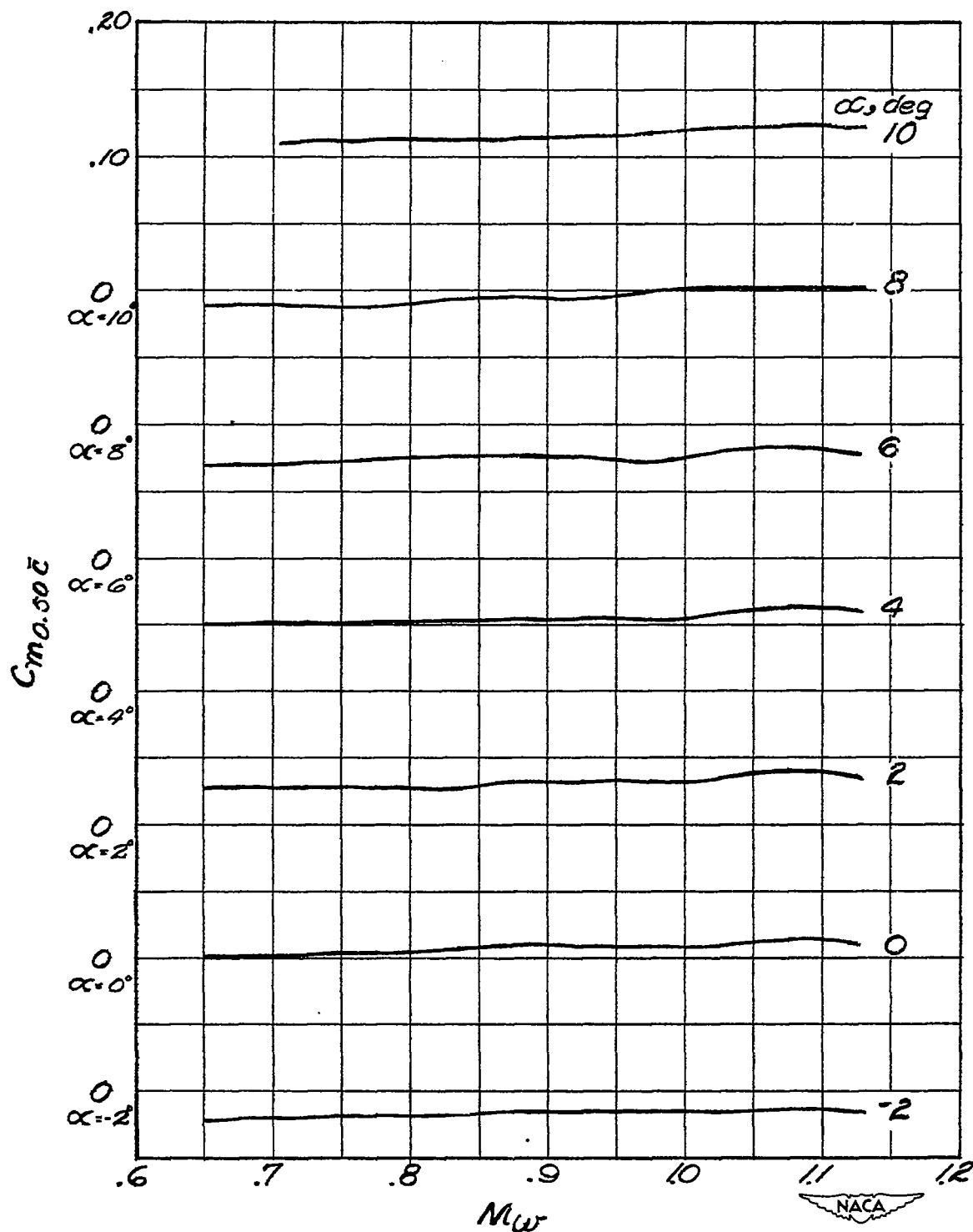


Figure 17.- Variation of pitching-moment coefficient with Mach number at various angles of attack for the fuselage alone.

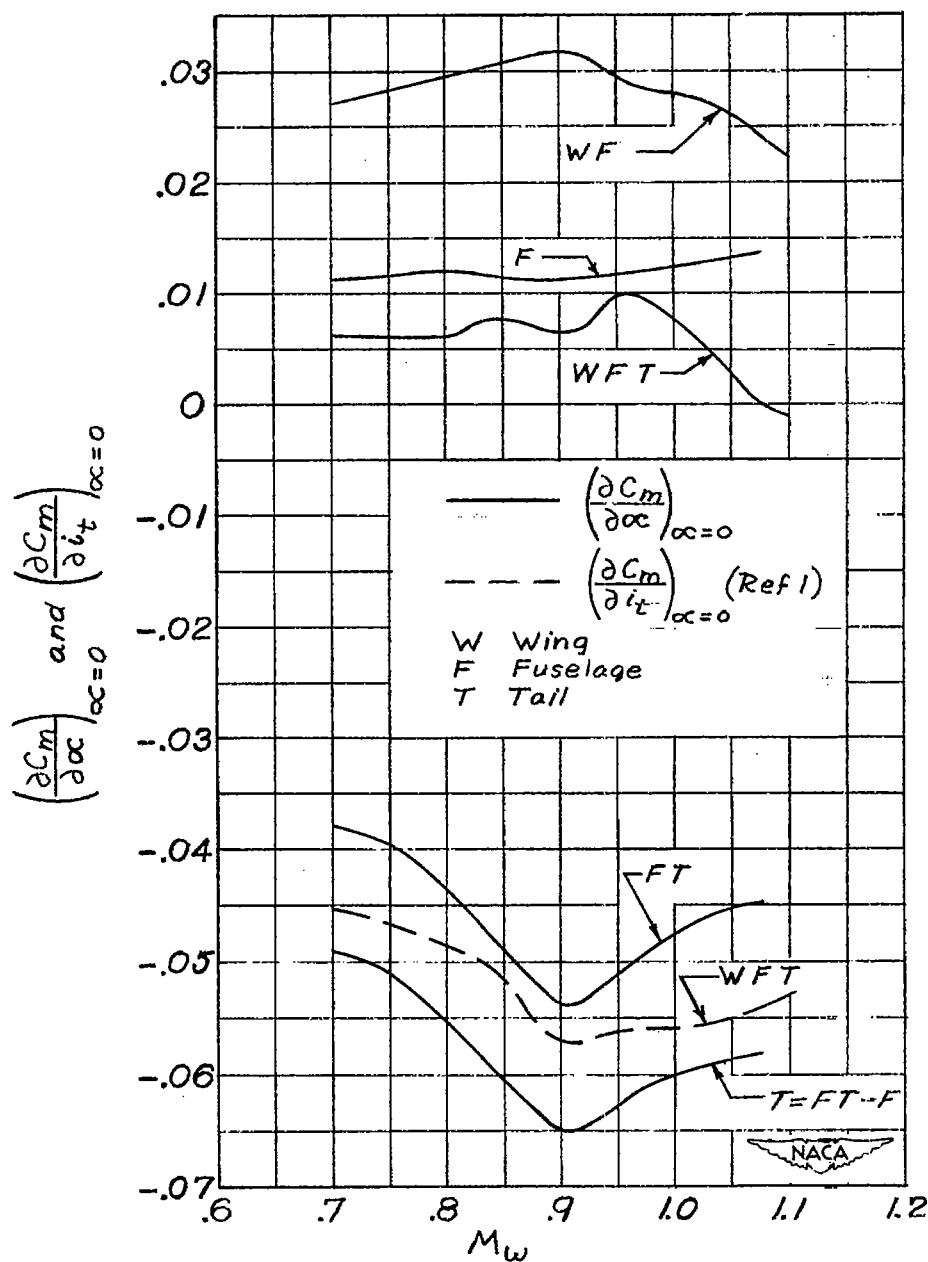


Figure 18.- Variations with Mach number of rate of change of pitching-moment coefficient with angle of attack $\left(\frac{\partial C_m}{\partial \alpha}\right)_{\alpha=0}$ for various model combinations. Variation with Mach number of rate of change of pitching-moment coefficient with stabilizer incidence $\left(\frac{\partial C_m}{\partial i_t}\right)_{\alpha=0}$ for complete model also shown.

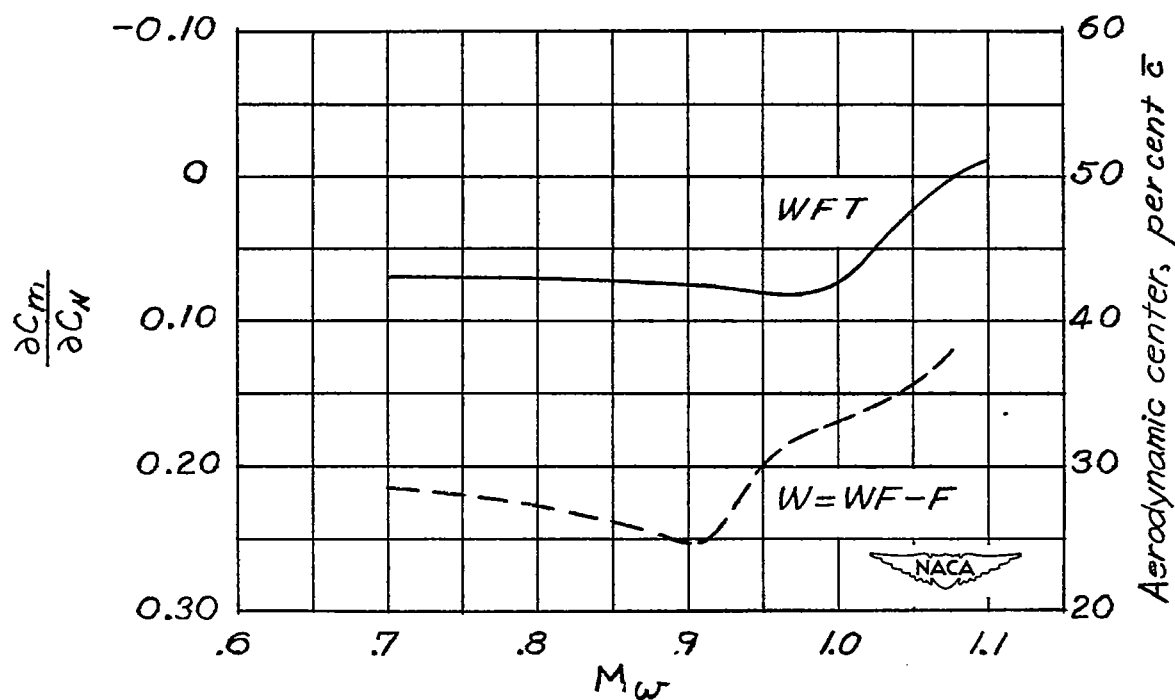




Figure 19.- Variation of $\frac{\partial C_m}{\partial C_N}$ with Mach number for complete model and wing alone plus wing-fuselage interference. Scale for aerodynamic center also given.

~~CONFIDENTIAL~~

NACA RM L51E01

	Symbol	Planform	\bar{c}	S	$b/2$	A	Reference
Experimental	\odot		1.79	.041	3.44	4.0	Present Tests
Theoretical	---		1.79	.041	3.32	3.7	3

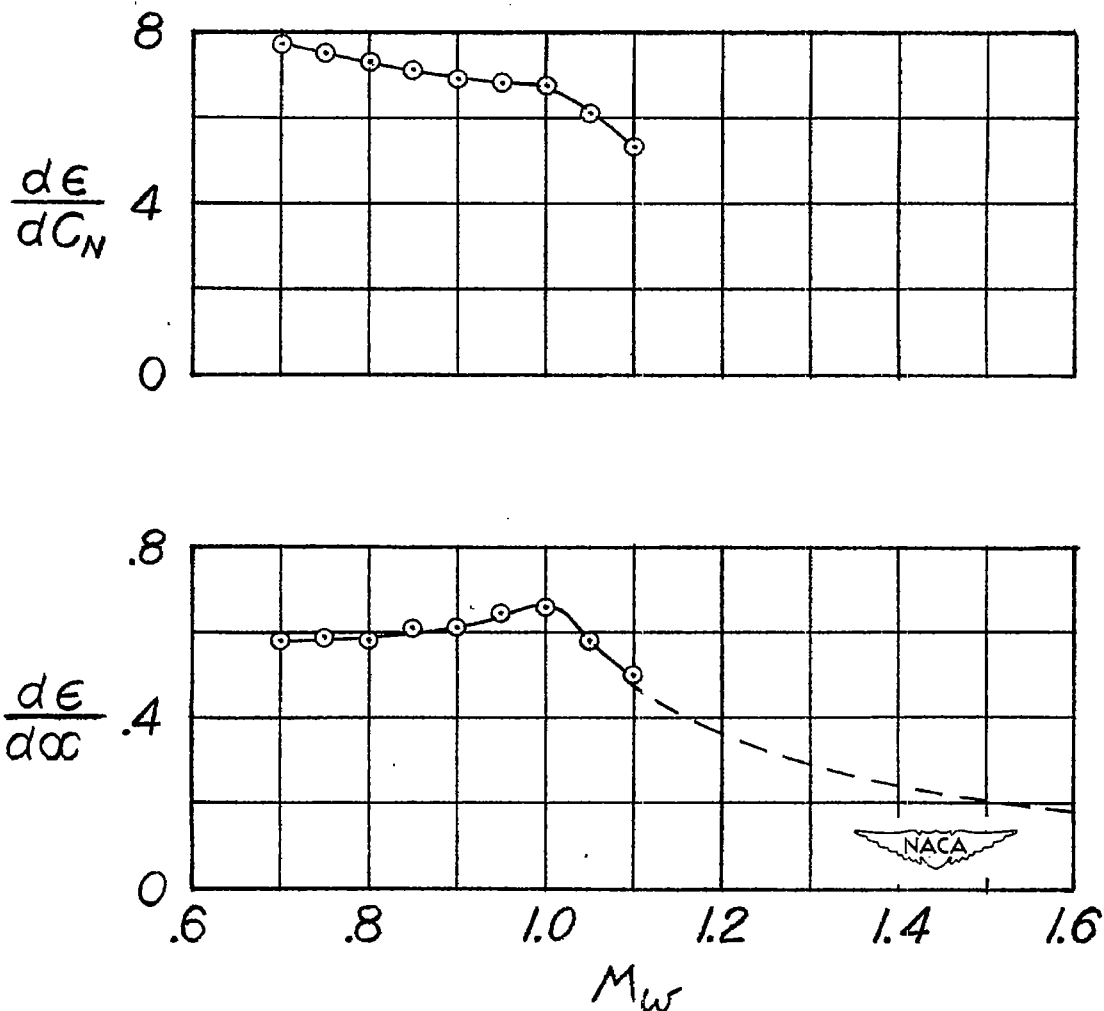


Figure 20.- Variation of $d\epsilon/dC_N$ and $d\epsilon/d\alpha$ with Mach number. Theoretical curve of $d\epsilon/d\alpha$ shown for rectangular wing of same area and mean aerodynamic chord.

~~CONFIDENTIAL~~